Eur. Phys. J. B **25**, 11–17 (2002)
DOI: 10.1140/e10051-002-0002-1

THE EUROPEAN PHYSICAL JOURNAL B
EDP Sciences

Metal nanocluster formation in silica films prepared by rf-sputtering: an experimental study

S. Padovani[1], F. D'Acapito[2], E. Cattaruzza[3], A. De Lorenzi[3], F. Gonella[3,a], G. Mattei[1], C. Maurizio[1], P. Mazzoldi[1], M. Montagna[4], S. Ronchin[4], C. Tosello[4], and M. Ferrari[5]

[1] INFM, Dipartimento di Fisica, Università di Padova, via Marzolo 8, 35131 Padova, Italy
[2] INFM, European Synchrotron Radiation Facility, GILDA-CRG, BP 220, 38043 Grenoble, France
[3] INFM, Dipartimento di Chimica Fisica, Università di Venezia, Dorsoduro 2137, 30123 Venezia, Italy
[4] INFM, Dipartimento di Fisica, Universitá di Trento, 38050 Povo-Trento, Italy
[5] CNR-CeFSA, Centro Fisica Stati Aggregati, 38050 Povo-Trento, Italy

Received 29 June 2001

Abstract. Composite silica films containing metal nanoclusters were prepared by the rf- sputtering technique, in which SiO_2 was co-deposited with gold+copper, gold+silver, or copper+silver. The formation of either pure or alloy clusters was studied by extended X-ray absorption fine structure spectroscopy and transmission electron microscopy. For all systems, the presence of alloy aggregates was evidenced. Moreover, small amounts of pure metal aggregates as well as dispersed or oxidized dopants were observed.

PACS. 61.46.+w Nanoscale materials: clusters, nanoparticles, nanotubes, and nanocrystals – 61.10.Ht X-ray absorption spectroscopy: EXAFS, NEXAFS, XANES, etc. – 81.05.Pj Glass-based composites, vitroceramics

1 Introduction

Silica-based composite materials containing metal nanoclusters are attractive since they are expected to exhibit features that can be exploited in integrated-optical devices [1], owing to their transparency in the optical fibers transmission window. The possibility of obtaining prescribed material features by tailoring the clusters structure in terms of composition and size distribution has motivated the investigation of various preparation methodologies for these composites. Sputtering deposition technique is particularly suitable for co-depositing the matrix together with more than one dopant element, so possibly creating core-shell or alloy aggregates [2–5]. Moreover, by sputtering deposition one can prepare homogeneous films several microns thick, so operating in the field of light waveguiding structures. In order to obtain a complete information on the structure of the composite systems, extended X-ray absorption fine structure (EXAFS) spectroscopy and transmission electron microscopy (TEM) analysis were performed. In particular, EXAFS spectroscopy has been demonstrated to be very suitable for investigating metal nanocluster composite glasses [6–8], especially when cluster of binary alloys may have formed for which the lattice parameters of the two single pure metals are similar, as for Au and Ag.

[a] e-mail: gonella@unive.it

2 Experimental procedure

The deposition of the samples was performed by means of a radio frequency sputtering apparatus. The residual pressure, before deposition, was about 2×10^{-7} mbar. The substrates used in each deposition run were silica slabs (25×75 mm^2 size). During deposition the substrates were not heated. The sputtering was carried out for 3 hours with an ultra pure Ar gas at a pressure of 7×10^{-3} mbar. The applied rf power was 150 W with a reflected power of 18 W. The deposition was carried out by putting on the target disk of silica (100 mm diameter) some pieces of the different couples of metals (Au-Cu, Au-Ag, Cu-Ag). After the deposition, the samples were heat-treated in air for 1 hour at 250 °C in order to remove defects; low temperature was chosen to prevent the cluster formation and aggregation (at 250 °C, the grown of Ag cluster was not observed [2]). In the following, samples are labeled AuCu, AuAg and CuAg. In this paper we also show the effect of an annealing in air at 700 °C for the sample containing Au and Cu (sample labeled AuCu-h).

EXAFS measurements were performed at the European Synchrotron Radiation Facility (ESRF) on the Italian beamline GILDA, with a bending magnet device source. The sagittally focusing monochromator, used in the so-called dynamical focusing mode [9], was equipped with two Si(311) crystals. The flux on the sample was of the order of 1×10^{10} photons s^{-1}. Spectra were recorded in

fluorescence mode, at liquid nitrogen temperature, at the Cu and Ag K-edges and at the Au LIII-edge. The signal collection was achieved by a high-purity 13-element Ge detector, keeping the total count rate per single element below 2×10^4 cps, to assure linear response. Reference spectra were also collected at 77 K in transmission mode for Cu, Ag and Au foils.

Transmission electron microscopy (TEM) characterization was performed with a Philips CM30 microscope operating at 300 kV, equipped with an EDAX energy-dispersive X-ray spectrometer (EDS) at the CNR-LAMEL Institute in Bologna. The samples for electron microscopy were prepared in cross section. To prevent sample damage and artifacts induced by temperature rise during ion milling, the specimens were cryogenically cooled at liquid nitrogen temperature. For localized EDS measurement on a single cluster a nanoprobe of nominal 8 nm FWHM was used.

3 Results and discussion

After deposition and annealing, nanocluster formation was evidenced for all systems by transmission electron microscopy. The thickness of the deposited films were obtained from TEM cross-sectional bright-field image, varying from 3 to 3.7 μm.

EXAFS data analysis was performed by Fourier filtering and multiparameter fit of first coordination shell in R-space; theoretical scattering amplitudes and phases were generated using the FEFF8 code [10] in the hypothesis of an fcc solid solution of binary alloy of AuAg, CuAg and AuCu for the respective samples. Fitting procedure was performed at the same time for both dopant edges. For any couple of different metals, the same intermetallic distance and Debye-Waller factor were supposed. The multi-electron amplitude reduction factor S_0^2 in standard EXAFS formula was fixed to the value obtained from the correspondent metal spectrum measured at the same edge. The values of S_0^2 parameters, calculated from a first shell fit of the metal standard spectrum, are 0.9 for both Cu and Ag cores and 1.1 for Au core. For CuAg and AuAg samples, a refinement of the fitting procedure was performed, considering a non Gaussian distribution of interatomic distances [11,12]. In the analysis of these two samples, it was necessary to introduce the third cumulant C_3 since the Gaussian model lead to unphysical low values of bond lengths, following an approach already used for similar systems like bulk AuNi [13].

Figure 1 shows the EXAFS spectra of the samples together with the signals from pure Au, Cu and Ag foils measured in transmission mode. Figure 2a, b, c shows the moduli of Fourier transform at the three edges for the samples and for the corresponding metal standard. For all samples, the peak located at about 2.3 Å corresponds to an intermetallic correlation. Moreover, the signal features of the spectra and the corresponding metal standards indicate that most of the nanocrystals are made of both the metal dopants. The experimental data for the sputtered films are shown together with the respective fit.

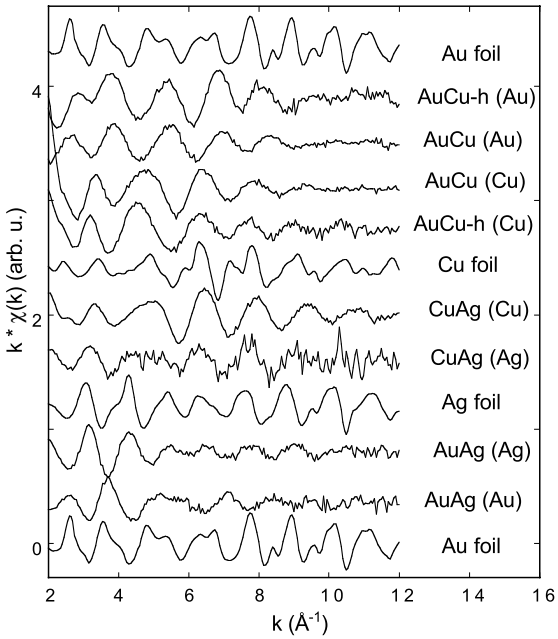

Fig. 1. EXAFS spectra of the examined samples (in brackets the respective edge), together with spectra for pure metal standard foils (different scales).

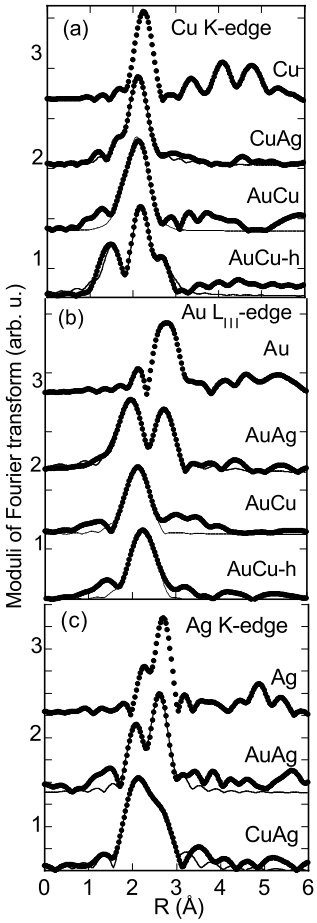

Fig. 2. Moduli of Fourier transform of EXAFS spectra (dots: experimental, solid line: fit), compared with the respective standard spectrum at (a): Cu K-edge, (b): Au LIII-edge, (c): Ag K-edge. EXAFS spectra are either k2- or k3-weighted, and transformed in the 2.5–12 $Å^{-1}$ k- range.

Table 1. Results of the EXAFS analysis: interatomic distance R, coordination number N, Debye-Waller factor σ^2 and third cumulant C_3 values are shown. For the standard metallic foils, the values of R and N are taken from reference [15], while the Debye-Waller values come from fit results.

sample	edge	elements	R (Å)	N	σ^2 (10^{-3} Å^2)	C_3 (10^{-4} Å^3)
Cu	K		2.5561	12	4	-
Au	L_{III}		2.8837	12	4	-
Ag	K		2.8894	12	4	-
	Cu K	Cu-Cu	2.46 ± 0.02	1 ± 1	14 ± 2	-
AuCu		Cu-Au	2.55 ± 0.02	4 ± 1	14 ± 2	-
	Au L_{III}	Au-Cu	2.55 ± 0.02	5 ± 1	14 ± 2	-
		Cu-O	1.91 ± 0.02	0.8 ± 0.6	3 ± 6	-
AuCu-h	Cu K	Cu-Cu	2.54 ± 0.02	0.8 ± 0.6	6 ± 5	-
		Cu-Au	2.64 ± 0.02	4 ± 1	16 ± 2	-
	Au L_{III}	Au-Cu	2.64 ± 0.02	6 ± 1	16 ± 2	-
	Cu K	Cu-Cu	2.51 ± 0.04	9 ± 3	16 ± 4	11 ± 10
CuAg		Cu-Ag	2.70 ± 0.04	1.5 ± 0.5	4 ± 2	11 ± 4
	Ag K	Ag-Cu	2.70 ± 0.04	2.0 ± 0.6	4 ± 2	11 ± 4
		Ag-Ag	2.87 ± 0.14	3 ± 5	17 ± 19	-
	Au L_{III}	Au-Au	2.74 ± 0.04	6 ± 2	12 ± 3	18 ± 7
AuAg		Au-Ag	2.93 ± 0.13	1.4 ± 0.4	10 ± 9	75 ± 6
	Ag K	Ag-Au	2.93 ± 0.13	2 ± 3	10 ± 9	41 ± 19
		Ag-Ag	2.81 ± 0.10	3 ± 2	11 ± 3	-

Experimental data are generally well fitted for all the examined systems. First-shell fitting results are reported in Table 1, which summarizes coordination number N, interatomic distance R, Debye-Waller parameter σ^2, and third cumulant C_3 (where used) for all the three cases. Debye-Waller factors are generally larger than bulk values, because the examined systems are more complex and intrinsically more disordered.

EXAFS fitting results for AuCu sample indicate the presence of Au:Cu alloy nanoclusters and Cu-Cu coordination. The formation of alloy structures was evidenced for both the edges by the presence of a contribution of the other metal. The interatomic distances result contracted with respect to the bulk ones; this suggest that the presence of small clusters, evidenced by TEM analysis, is accompanied by few-atoms structures, that are known to exhibit similar contracted interatomic distances [14]. Low coordination number is due to the cluster size and to atoms dispersed in the silica matrix. For this sample, the third cumulant can be neglected. Figure 3 (left) shows the bright-field TEM cross-section of the sample AuCu: uniformly distributed spherical clusters are found throughout the interested layer, with average diameter $D = 1.4 \pm 0.5$ nm (mean diameter with standard deviation), as reported in the histogram of the size distribution of Figure 4 (upper).

From EDS analysis, the atomic ratio [Au]/[Cu] measured for the whole sample is 0.34 ± 0.04, a value that confirms the higher Cu concentration as from EXAFS analysis (see Tab. 1).

Results of fitting procedures for AuCu-h sample are consistent with the presence of metallic copper ($R_{\text{Cu-Cu}}$ is similar to the bulk value [15]), together with $Au_{0.25}Cu_{0.75}$ alloy nanoclusters (Vegard distance [16] $R_{\text{Cu-Au}} = 2.6495$ Å) and copper atoms coordinated by oxygens at

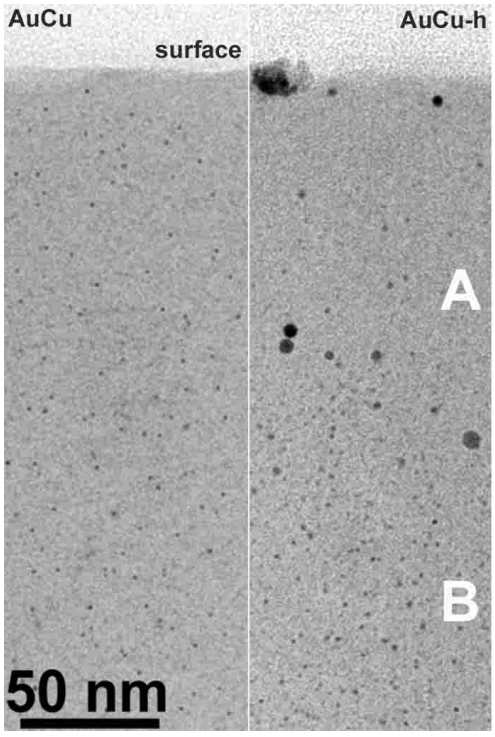

Fig. 3. Bright-field TEM cross section of: (left panel) AuCu sample, (right panel) AuCu-h sample.

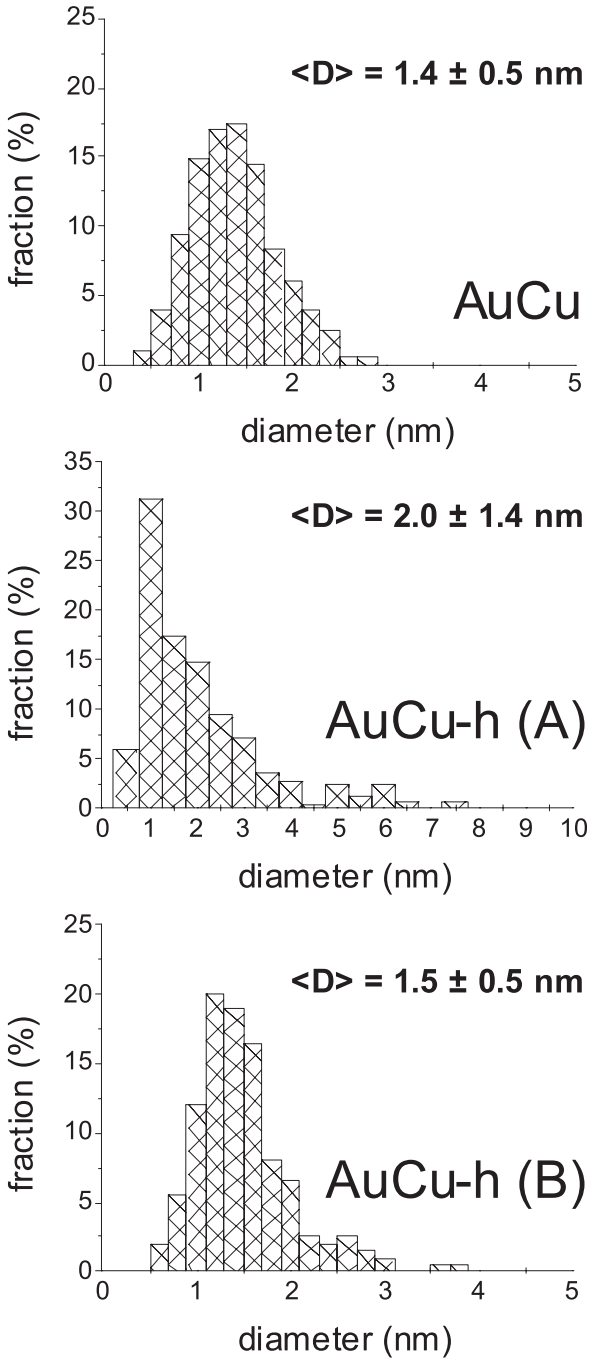

Fig. 4. Histogram of the size distribution for: (upper panel) AuCu sample, (middle panel) zone A of AuCu-h sample (see Fig. 3) and (lower panel) zone B of AuCu-h sample (see Fig. 3).

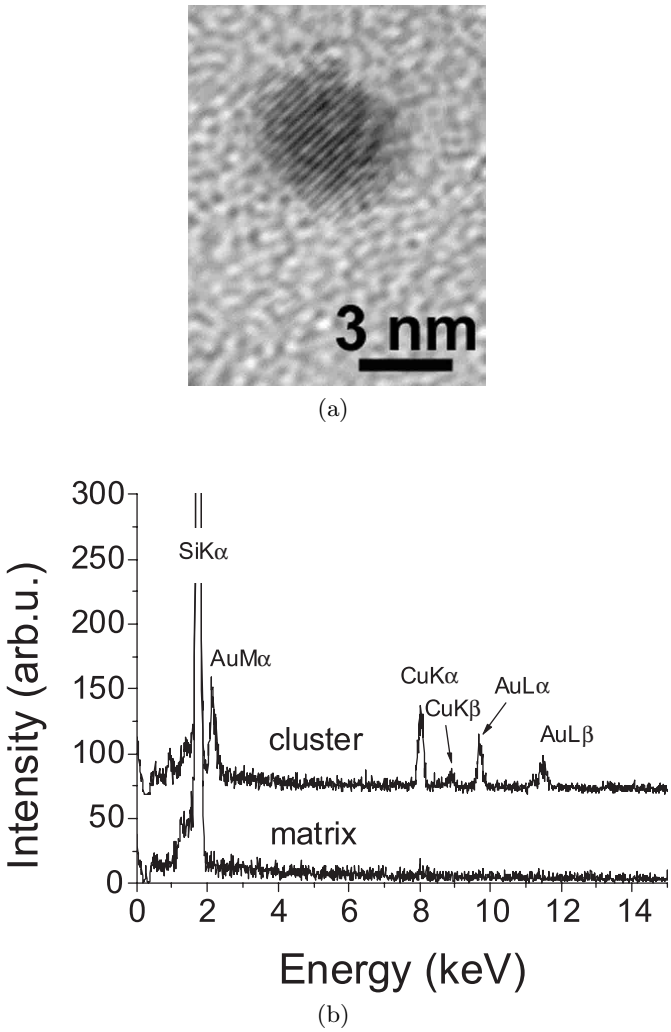

Fig. 5. (a) High Resolution TEM image of a cluster in AuCu-h sample; (b) EDS measurement on a cluster and on the surrounding matrix.

a mean distance $R_{\text{Cu-O}} = 1.91$ Å, comparable to the CuO bulk value of 1.947 Å [15]. Low metal coordination number from Cu K-edge analysis is due to both small cluster size and to the presence of Cu atoms in oxide phase. Low coordination number resulting from the analysis at Au L_{III}-edge is due to the cluster size and to gold atoms dispersed in the silica matrix. Also in the analysis for this sample, the third cumulant can be neglected. With respect to the sample annealed at 250 °C, interatomic distances and coordination numbers increase, according with the growth of the cluster diameter evidenced by TEM. Moreover, TEM analysis showed the presence of two morphologically different regions: a superficial one, (labeled A in the right panel of Fig. 3) about 150 nm thick, exhibits larger clusters with respect to the second one (labeled B), in which the size of the clusters is similar to that of the AuCu sample. This can be seen from the histograms of the size distribution for the AuCu and AuCu-h samples reported in Figure 4: a cluster diameter of $D = 2.0 \pm 1.4$ nm is found in region A of the AuCu-h sample(middle panel), while in region B (lower panel) the size is $D = 1.5 \pm 0.5$ nm, which is practically the same as the size distribution measured in the AuCu sample ($D = 1.4 \pm 0.5$ nm, upper panel). From the high resolution (HRTEM) image of a nanoparticle in the superficial region (Fig. 5a) one can see the crystalline structure of the cluster resulting from the interference of the (111) planes. EDS analysis, performed on one of these

clusters (Fig. 5b) and on the surrounding matrix, shows the presence of both Au and Cu in the cluster (with a [Au]/[Cu] atomic ratio of 0.9 ± 0.1) and that in this superficial layer the clusters are not surrounded by dispersed metal atoms. This is a clear indication of the AuCu alloy formation. The ratio [Au]/[Cu] measured by EDS for the whole sample is 0.82 ± 0.05, that – compared with the value 0.32 ± 0.04 measured in the AuCu sample – suggests that air annealing at 700 °C is able to promote Cu out-diffusion from the sample, with a modification of the local Au and Cu concentrations mostly in the surface layer (zone A). One can further understand this point, considering that EXAFS analysis, which averages over the whole thickness, gives a [Au]/[Cu] ratio of about 0.3, *i.e.*, similar to that in the AuCu sample, therefore indicating that alloy clusters in the deeper region of the AuCu-h sample were practically not affected by the annealing. This is in agreement with references [17,18], which show that air annealing in sequentially Au-Cu implanted or sol-gel Au-Cu co-doped silica results in a separation of the AuCu alloy followed by Cu migration toward the surface and oxidation. Indeed, at the surface of AuCu-h samples TEM analysis showed large aggregates (see right panel of Fig. 3), which by EDS analysis are found to contain Cu.

EXAFS fitting results for AuAg sample indicate the presence of Au:Ag alloy nanoclusters. Since lattice parameters of metallic Au and Ag are the same within 1/100 Å, diffraction techniques are not suitable to evidence Au:Ag alloy, because of the peak broadening peculiar of such small clusters. On the contrary, EXAFS spectroscopy can easily distinguish the two species from the different backscattering amplitude functions. It should be noted that measured $R_{Au\text{-}Au}$ and $R_{Ag\text{-}Ag}$ are contracted with respect to the corresponding bulk values by few percents. This result, together with the low coordination numbers, attests the presence of few-atoms structures, that are known to exhibit similar contracted interatomic distances [19,20]. The left panel of Figure 6 shows the bright-field TEM cross-section of the sample AuAg: uniformly distributed spherical clusters are evident throughout the interested layer, with average diameter $D = 1.5 \pm 0.5$ nm as deduced from the histogram of the size distribution of Figure 7. From EDS measurement, the ratio [Ag]/[Au] for the whole sample is 1.8 ± 0.3.

CuAg sample presents metallic clusters, which from EXAFS analysis result to be composed part of both Cu and Ag, and part of single metal structures: $R_{Cu\text{-}Ag}$ is intermediate between Cu and Ag metal phase. It should be underlined that Ag:Cu alloy is not thermodynamically predicted for bulk system [21]. Recently, silica doping by sequential ion implantation of Cu and Ag [22] showed that the two metallic species precipitate separately to form pure Ag and Cu nanocrystals, indicating the crucial role of the preparation method in giving different nanostructures. Moreover, the contraction of Cu-Cu interatomic distance [14] (see Tab. 1) with respect to the bulk value is likely due to the formation of low dimensional systems (*e.g.*, polyatomic chains) as in the case of AuAg sample. Results of fitting procedure for Ag K-edge are consistent

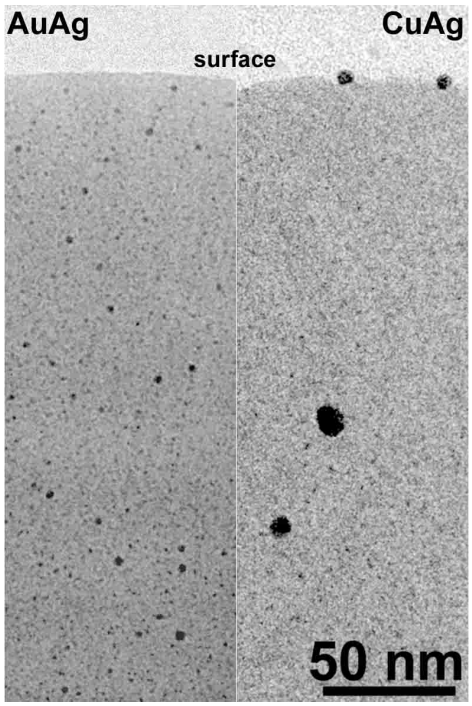

Fig. 6. Bright-field TEM cross section for: (left panel) AuAg sample and (right panel) CuAg sample.

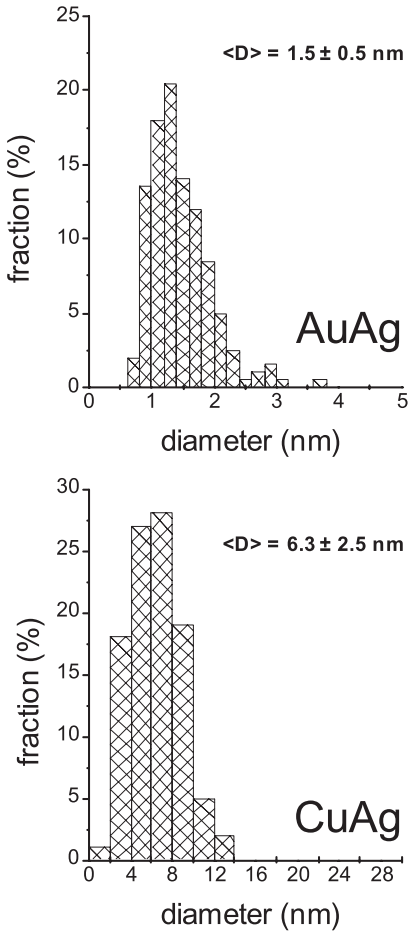

Fig. 7. Histogram of size distribution for: (upper panel) AuAg sample and (lower panel) CuAg sample.

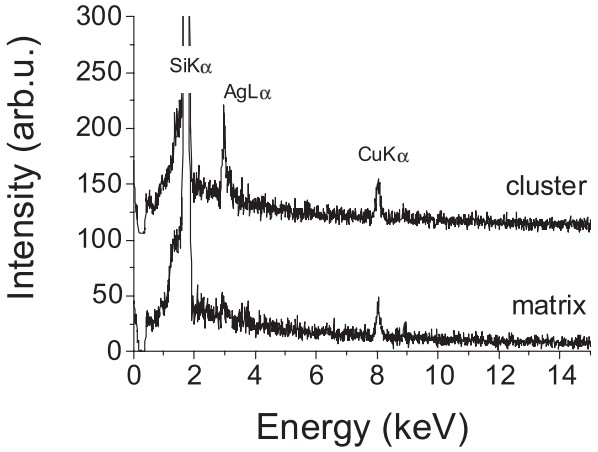

Fig. 8. EDS spectrum for CuAg sample, (a) on a region containing one cluster and (b) from the surrounding matrix.

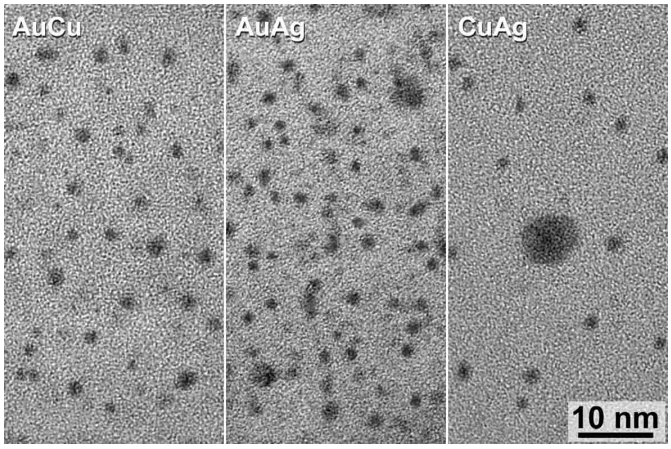

Fig. 9. Bright-field TEM cross section at higher magnification for the samples: (left panel) AuCu, (middle panel) AuAg and (right panel) CuAg sample.

with the presence of metallic silver clusters ($R_{Ag\text{-}Ag}$ is similar to the bulk value [15]). Figure 6 (right panel) shows the TEM image of the sample: a bimodal size distribution is evident, for which large clusters, 6.3 ± 2.5 nm of average diameter (Fig. 7b), are dispersed together with small (about 1 nm of average diameter) ones. While EDS analysis on the whole sample indicates a ratio [Cu]/[Ag] of 1.3 ± 0.2, a measurement on single clusters belonging to the population with the largest size, whose histogram is reported in Figure 7b, reveals the presence of both silver and copper (with a strong predominance of Ag), while a small amount of copper is present on the surrounding matrix (Fig. 8). A comparison of the nanostructure of the cluster in all the sample investigated is reported in the TEM cross- sectional bright-field of Figure 9.

It must be remarked that the thermodynamics related to the nanoaggregatation in an alloy form should be carefully used especially when dealing with the Cu:Ag systems, where the bulk alloy formation does not occur. Recently, Jesser *et al.* [23] studied the phase diagram dependence of binary alloys on the nanocluster size, showing that some physical parameters may undergo a dramatic change, for example, the solubility may increase by a factor of ten (case of Bi:Sn system). In general, as discussed in details by Hagège *et al.* [24], the solubility of two species in the nanocluster depends on the relative magnitudes of the interface energies between the two alloy components and the surrounding matrix. This means that the dimension of a particle plays a fundamental role in the definition of its thermodynamic behavior in terms of the possible structures. Indeed, the formation of either core-shell structures or bimetal spheres with a planar interface between the two constituents gives rise to a different energy balance, depending on the interface/volume ratio for both metal/metal and metal/matrix couples. The calculation for the alloy formation must therefore take into account all these situations depending on the particle size. In the case discussed in this work, the cluster size distribution is not sufficiently narrow to allow a reliable estimation. Moreover, EXAFS results evidence the presence of different phases in the same sample region, preventing the effectiveness of thermodynamic considerations for the examined systems. Work is progress to refine the preparation methodology with the aim to obtain narrow size distributions for the nanoaggregates.

4 Conclusions

In conclusion, rf-sputtering deposition technique has demonstrated to be suitable for the preparation of binary metal nanoclusters in silica matrix. The experimental results indicate that a variety of different structures can form, depending on the used elements as well as on the treatment parameters. In particular, the possible formation of thermodynamically unfavourable mixtures has been evidenced by EXAFS analyses in the case of CuAg systems. Study is in progress to investigate how the observed cluster size, size distribution and composition are determined mainly by the local dopants concentration, and how – on the other hand – the preparation route could play an effective role in giving a particular structure.

References

1. F. Gonella, P. Mazzoldi, *Metal Nanocluster Composite Glasses*, in: *Handbook of Nanostructured Materials and Nanotechnology*, edited by H.S. Nalwa, Vol. 4 (Academic Press, S. Diego, 2000), pp. 81–158.
2. I. Tanahashi, M. Yoshida, Y. Manabe, T. Tohda, J. Mater. Res. **10**, 362 (1995).
3. T. Akai, H. Yamanaka, H. Wakabayashi, J. Am. Ceram. Soc. **79**, 859 (1996).
4. I. Tanahashi, Y. Manabe, T. Tohda, S. Sasaki, A. Nakamura J. Appl. Phys. **79**, 1244 (1996).
5. C. Tosello, S. Ronchin, E. Moser, M. Montagna, P. Mazzoldi, F. Gonella, M. Ferrari, C. Duverger, R. Belli, G. Battaglin, Phil. Mag. B **79**, 2103 (1999).

6. F. D'Acapito, S. Mobilio, F. Gonella, C. Maurizio, P. Mazzoldi, G. Battaglin, E. Cattaruzza, F. Zontone, Eur. Phys. J. D **10**, 123 (2000).
7. F. Gonella, E. Cattaruzza, G. Battaglin, F. D'Acapito, C. Sada, P. Mazzoldi, C. Maurizio, G. Mattei, A. Martorana, A. Longo, F. Zontone, J. Non-Cryst. Solids **280**, 214 (2001).
8. F. D'Acapito, G. Battaglin, F. Caccavale, E. Cattaruzza, F. Gonella, P. Mazzoldi, S. Mobilio, J.R. Regnard, J. Appl. Phys. **87**, 1819 (2000).
9. S. Pascarelli, F. Boscherini, F. D'Acapito, J. Hrdy, C. Meneghini, S. Mobilio, J. Synchr. Rad. **3**, 147 (1996).
10. A.L. Ankudinov, B. Ravel, J.J. Rehr, S.D. Conradson, Phys. Rev. B **58**, 7565 (1998).
11. P. Eisenberger, G.S. Brown, Solid State Commun. **29**, 481 (1979).
12. J.M. Tranquada, R. Ingalls, Phys. Rev. B **28**, 3520 (1983).
13. G. Renaud, N. Motta, F. Lancon, M. Belakhovsky, Phys. Rev. B **38**, 5944 (1988).
14. P.A. Montano, G.K. Shenoy, E.E. Alp, W. Schulze, J. Urban, Phis. Rev. Lett. **56**, 2076 (1985).
15. R.N.G. Wychoff, *Crystal Structures* (Wiley, New York, 1964).
16. P. Villars, L.D. Calvet, *Pearson's Handbook of Crystallographic Data* (ASM International, Materials Park, OH, 1991).
17. F. Gonella, G. Mattei, P. Mazzoldi, C. Sada, G. Battaglin, E. Cattaruzza, Appl. Phys. Lett. **75**, 55 (1999).
18. G. De, G. Mattei, P. Mazzoldi, C. Sada, G. Battaglin, A. Quaranta, Chem. Mater. **12**, 2157 (2000).
19. P.A. Montano, J. Zaho, M. Ramanathan, G.K. Shenoy, W. Schulze, J. Urban, Chem. Phys. Lett. **164**, 126 (1989).
20. S. Mobilio, G. D'Agostino, A. Pinto, Phys. Rev. B **48**, 14447 (1993).
21. T.B. Massalski, *Binary Alloy Phase Diagrams I*, edited by J.L. Murray, L.H. Bennett, H. Baker (ASM International, Materials Park, OH, 1987).
22. P. Mazzoldi *et al.* (in preparation).
23. W.A. Jesser, G.J. Shiflet, G.L. Allen, J.L. Crawford, Mat. Res. Innovat. **2**, 211 (1999).
24. S. Hagège, U. Dahmen, Phil. Mag. Lett. **74**, 259 (1996).